

## Supporting Information

### **Tuning the RE-UiO-66 metal–organic framework platform for white light emission**

Zvart Ajoyan,<sup>‡ab</sup> Hudson A. Bicalho,<sup>‡ab</sup> P. Rafael Donnarumma,<sup>ab</sup> Artsiom Antanovich,<sup>c</sup>  
and Ashlee J. Howarth<sup>\*ab</sup>

<sup>a</sup> Department of Chemistry and Biochemistry and Centre for NanoScience Research,  
Concordia University, 7141 Sherbrooke Street West, Montréal, Quebec H4B 1R6,  
Canada.

<sup>b</sup> FRQNT Quebec Centre for Advanced Materials (QCAM/CQMF), Montréal, Canada.

<sup>c</sup> Department of Physical Chemistry, Technische Universität Dresden, Zellescher Weg  
19, 01069, Dresden, Germany.

## **Experimental details**

### **Materials**

All chemicals were used as received from commercial sources. *N,N*-dimethylformamide (DMF), *N,N*-dimethylacetamide (DMA), and acetone were purchased from Fisher Scientific (Fisher Chemical). 2,6-Difluorobenzoic acid (2,6-DFBA) was purchased from AmBeed. Terbium(III) nitrate hydrate ( $\text{Tb}(\text{NO}_3)_3 \cdot x\text{H}_2\text{O}$ ), europium(III) nitrate hydrate ( $\text{Eu}(\text{NO}_3)_3 \cdot x\text{H}_2\text{O}$ ) and gadolinium(III) nitrate hydrate ( $\text{Gd}(\text{NO}_3)_3 \cdot x\text{H}_2\text{O}$ ) were purchased from Alfa Aesar. Terephthalic acid ( $\text{H}_2\text{BDC}$ ) was purchased from Acros Organics.

### **Methods**

Powder X-ray diffraction (PXRD) patterns were collected on a Bruker D8 Advance diffractometer (measurements made over a range of  $4^\circ < 2\theta < 40^\circ$  in  $0.02^\circ$  step with a 0.500 s scanning speed) equipped with a LYNEXE linear position sensitive detector (Bruker AXS, Madison, WI). Neat samples were smeared directly onto the silicon wafer of a propriety low-zero background sample holder. Data was collected using a continuous coupled  $\theta/2\theta$  scan with  $\text{CuK}\alpha$  ( $\lambda = 1.54178 \text{ \AA}$ ) radiation source.

Single-crystal X-ray diffraction (SCXRD) data for Tb:Gd:Eu-UiO-66 was collected on a Bruker D8 Venture diffractometer equipped with a Photon 200 area detector, and  $1\mu\text{S}$  microfocus X-ray source (Bruker AXS,  $\text{CuK}\alpha$  source). Structure solution was performed using SHELXTL software from Bruker.<sup>1</sup> The parameters were refined for all data by full-matrix-least squares or  $F^2$  using SHELXL.<sup>2</sup> It is important to mention that disordered molecules (including water, DMA, and dimethylammonium) in the MOF pores, which could not be reliably modelled using discrete atoms, were subtracted through the SQUEEZE method as part of PLATON package.<sup>3</sup> All of the nonhydrogen atoms were refined with anisotropic thermal parameters. Hydrogen atoms were placed in calculated positions and allowed to ride on the carrier atoms. All hydrogen atom thermal parameters were constrained to ride on the carrier atom. The crystal exhibits a strong diffuse scattering in the form of diffuse Bragg peaks and scattering between them. We believe that this is the source of high electron density on the metal centers.

MOF samples were activated using a Micromeritics SmartVacPrep instrument equipped with a hybrid turbo vacuum pump. Nitrogen adsorption-desorption isotherms were measured at 77K on a Micromeritics TriStar II Plus instrument.

Inductively coupled plasma mass spectrometry (ICP-MS) data was collected using an Agilent 7500 Series. ~0.5 mg of RE-UiO-66 was digested in 750  $\mu$ L H<sub>2</sub>SO<sub>4</sub> at 100 °C in a sand bath for 24 h. This solution was diluted with deionized H<sub>2</sub>O to a final volume of 10 mL.

Diffuse reflectance infrared Fourier transform spectroscopy (DRIFTS) data was recorded using a Thermo Scientific Nicolet 6700 FT-IR equipped with an MCT detector with a resolution of 1 cm<sup>-1</sup> in the range of 4000-450 cm<sup>-1</sup>. Prior to the analysis, the samples were activated and mixed with dry KBr.

Scanning electron microscopy (SEM) images and energy dispersive X-ray spectroscopy (EDS) data were collected on a Phenom ProX desktop SEM.

<sup>19</sup>F nuclear magnetic resonance (NMR) spectroscopy data were collected on a 500 MHz Varian spectrometer. Prior to the analysis, the sample was digested by adding 10 drops of D<sub>2</sub>SO<sub>4</sub> and 1 mL of DMSO-d<sub>6</sub>, followed by sonication for 5 minutes.

Diffuse Reflectance UV-Vis absorbance spectroscopy data were collected on a Cary 5 Series UV-Vis-NIR Spectrophotometer (Agilent Technologies) with the EasiDiff™ accessory. A 1 nm bandwidth and wavelength changeover at 350 nm were used for data collection. Activated samples were loaded into a sample cup mixed with potassium bromide.

Photoluminescence spectra were collected using a PTI QuantaMaster 8075 spectrofluorimeter (Horiba). Samples of RE-UiO-66 were suspended in dichloromethane and drop-cast on quartz slides prior to measurement.

To make a proof of concept white light emitting device, Tb:Gd:Eu-UiO-66 was coated onto a 310 nm 1 Watt UV LED as part of a XNiteFlashF Series Flashlight purchased from Llewellyn Data Processing. For that, the MOF sample was dispersed in dichloromethane and drop cast onto the UV LED chip.

Absolute photoluminescence quantum yield measurements were determined by using a Fluorolog-3 spectrofluorometer with a Quanta- $\phi$  integrating sphere (Horiba Jobin Yvon,

Inc.). For the measurements, powdered samples were deposited onto a glass slide covered with adhesive tape. Aluminum sulfate powder deposited in the same fashion was used as a blank sample.

Time resolved photoluminescence measurements were conducted at room temperature using a Horiba Jobin Yvon Fluorocube-01-NL under excitation with a NanoLED-350 pulsed laser diode ( $\lambda = 368$  nm, pulse duration 1.2 ns). For the measurements, powdered samples were deposited onto a glass slide covered with adhesive tape. To get a quantified value for the decay constants of all curves, the average lifetimes were used, calculated as:

$$\langle \tau \rangle = \frac{\sum_i B_i \tau_i^2}{\sum_j B_j \tau_j}$$

Photodegradation experiments were carried out by continuously irradiating a sample of Tb:Gd:Eu-UiO-66 drop cast on a quartz slide using 312 nm excitation. A new photoluminescence spectrum was collected every hour from 0–6 hours.

**Table S1.** The amounts of rare-earth metals used in the synthesis of single, bi- and tri-RE-UiO-66.

Sample	Measured Amounts (mg)			Measured Amounts (mmol)		
	Tb	Gd	Eu	Tb	Gd	Eu
Tb-UiO-66	78.9	-	-	0.174	-	-
Gd-UiO-66	-	78.5	-	-	0.174	-
Eu-UiO-66	-	-	77.6	-	-	0.174
Gd:Eu-UiO-66	-	70.6	8.2	-	0.1564	0.0183
Tb:Gd-UiO-66	20.9	61.1	-	0.0461	0.1353	-
Tb:Eu-UiO-66	63.9	-	20.2	0.1410	-	0.0452
Tb:Gd:Eu-UiO-66	17.8	52.0	5.4	0.0399	0.1183	0.0123

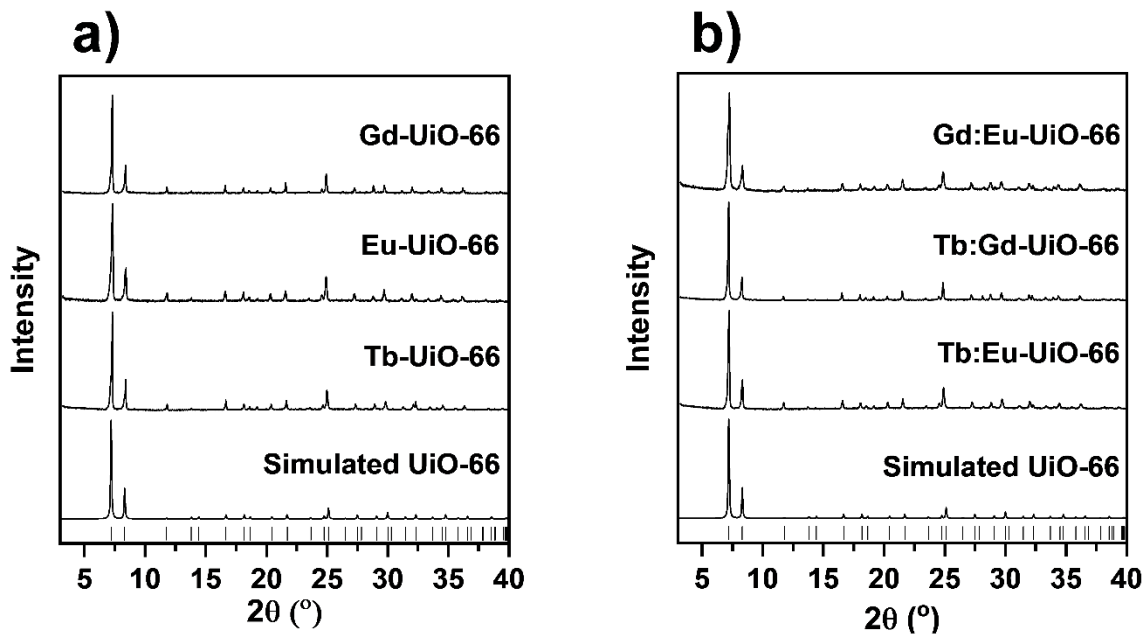


**Figure S1.** PXRD pattern for (a) as-synthesized Gd-UiO-66, Eu-UiO-66, and Tb-UiO-66 and the simulated pattern of Tb-UiO-66, and (b) as-synthesized Gd:Eu-UiO-66, Tb:Gd-UiO-66, and Tb:Eu-UiO-66 and the simulated pattern of Tb-UiO-66.

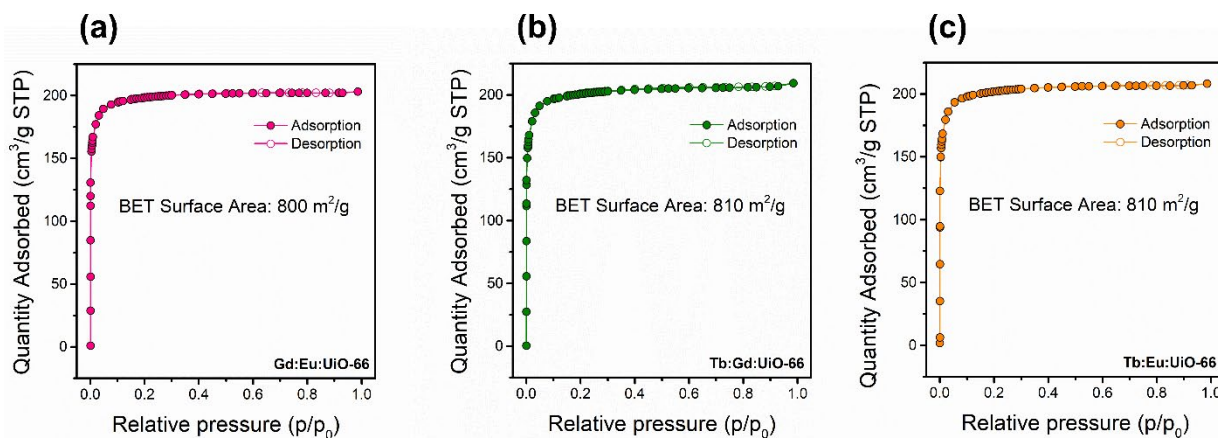


**Figure S2.** Nitrogen sorption isotherm for (a) Gd:Eu-UiO-66, (b) Tb:Gd-UiO-66 and (c) Tb:Eu-UiO-66.

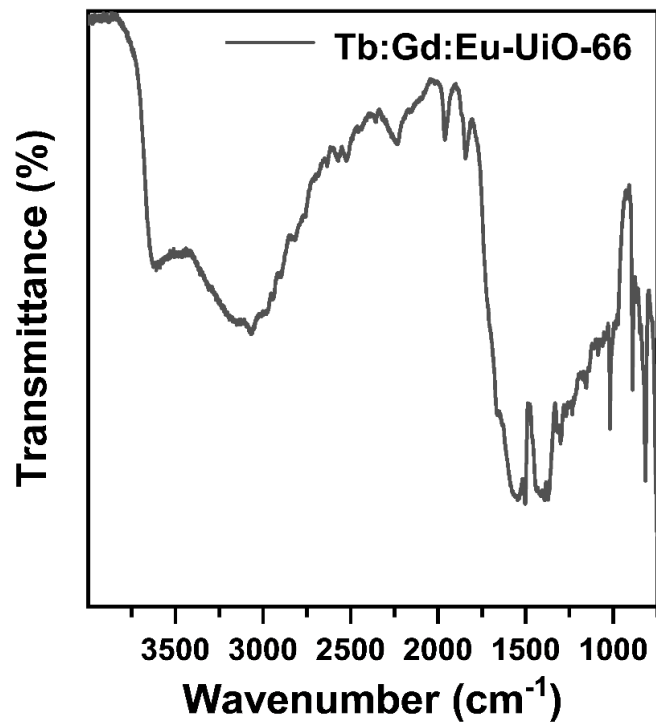


**Figure S3.** Diffuse reflectance infrared Fourier transform spectrum of Tb:Gd:Eu-Uio-66.

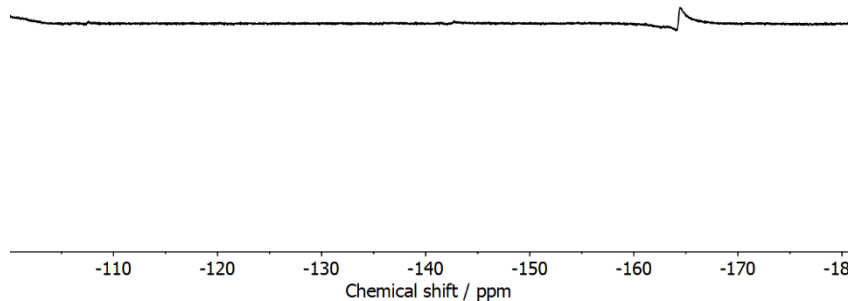


**Figure S4.** <sup>19</sup>F NMR spectrum of the digested Tb:Gd:Eu-Uio-66 MOF. The signal is weak due to the presence of Gd(III) in the sample which is paramagnetic and interferes with NMR spectroscopy.

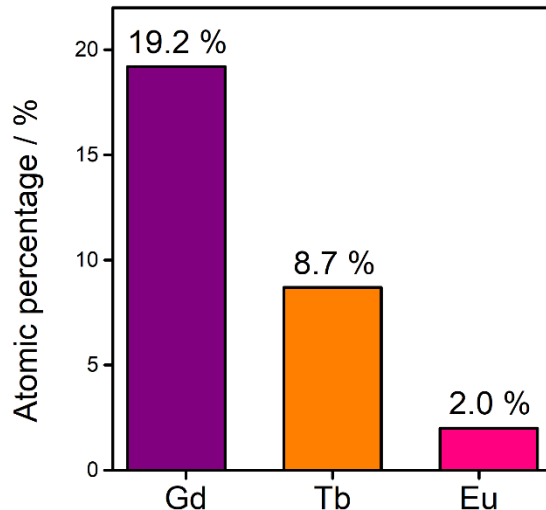


**Figure S5.** Atomic percentages of Gd(III), Tb(III) and Eu(III) in Tb:Gd:Eu-UiO-66. It is worth mentioning that these atomic percentages obtained by EDS exclude the presence of carbon in the sample, as a carbon tape was used for the sample preparation, so the carbon signal was suppressed to eliminate background noise.

In that way, the obtained percentages of 8.7, 19.2, and 2.0 % for Tb, Gd, and Eu would give a ratio of 1.7:3.9:0.4, respectively, considering the hexanuclear clusters in the RE-UiO-66 MOF, corroborating the results obtained by ICP-MS.

**Table S2.** ICP analysis of the metals in Tb:Gd:Eu-UiO-66.

Sample	ICP (molar ratio)			Measured Amounts (molar ratio)			Adjusted for Hexanuclear Cluster		
	Tb	Gd	Eu	Tb	Gd	Eu	Tb	Gd	Eu
Gd:Eu-UiO-66	-	8.5	1	-	8.5	1	-	5.4	0.6
Tb:Gd-UiO-66	1	2.8	-	1	2.9	-	1.6	4.4	-
Tb:Eu-UiO-66	3.5	-	1	3.1	-	1	4.6	-	1.4
Tb:Gd:Eu-UiO-66 (Batch 1)	3.6	9.7	1	2.9	9.5	1	1.5	4.1	0.4
Tb:Gd:Eu-UiO-66 (Batch 2)	3.6	9.5	1	3.0	9.6	1	1.5	4.1	0.4



**Figure S6.** Optical microscopy image of Tb:Gd:Eu single crystals upon UV light irradiation and taken under 10X magnification.

**Table S3.** Crystallographic data of Tb:Gd:Eu-UiO-66

<b>Crystal system</b>	Cubic
<b>Space group</b>	<i>Fm-3m</i>
<b><i>a</i>/Å</b>	21.6983(12)
<b><i>b</i>/Å</b>	21.6983(12)
<b><i>c</i>/Å</b>	21.6983(12)
<b><i>α</i>/°</b>	90
<b><i>β</i>/°</b>	90
<b><i>γ</i>/°</b>	90
<b>Volume/Å<sup>3</sup></b>	10215.9(17)
<b>Z</b>	1
<b><math>\rho_{\text{calc}}</math>/cm<sup>3</sup></b>	1.392
<b><math>\mu</math>/mm<sup>-1</sup></b>	24.218
<b>F(000)</b>	3965.0
<b>Crystal size/mm<sup>3</sup></b>	0.322 × 0.217 × 0.198
<b>Radiation</b>	CuK $\alpha$ ( $\lambda$ = 1.54178)
<b>2<math>\theta</math> range for data collection/°</b>	7.056 to 127.998
<b>Index ranges</b>	-24 ≤ <i>h</i> ≤ 24, -24 ≤ <i>k</i> ≤ 25, -25 ≤ <i>l</i> ≤ 23
<b>Reflections collected</b>	16170
<b>Independent reflections</b>	482 [ <i>R</i> <sub>int</sub> = 0.1632, <i>R</i> <sub>sigma</sub> = 0.0434]
<b>Data/restraints/parameters</b>	483/18/30
<b>Goodness-of-fit on F<sup>2</sup></b>	1.054
<b>Final R indexes [<i>I</i> ≥ 2<math>\sigma</math> (<i>I</i>)]</b>	<i>R</i> <sub>1</sub> = 0.0687, <i>wR</i> <sub>2</sub> = 0.2001
<b>Final R indexes [all data]</b>	<i>R</i> <sub>1</sub> = 0.0953, <i>wR</i> <sub>2</sub> = 0.2627
<b>Largest diff. peak/hole / e Å<sup>-3</sup></b>	3.75/-1.91

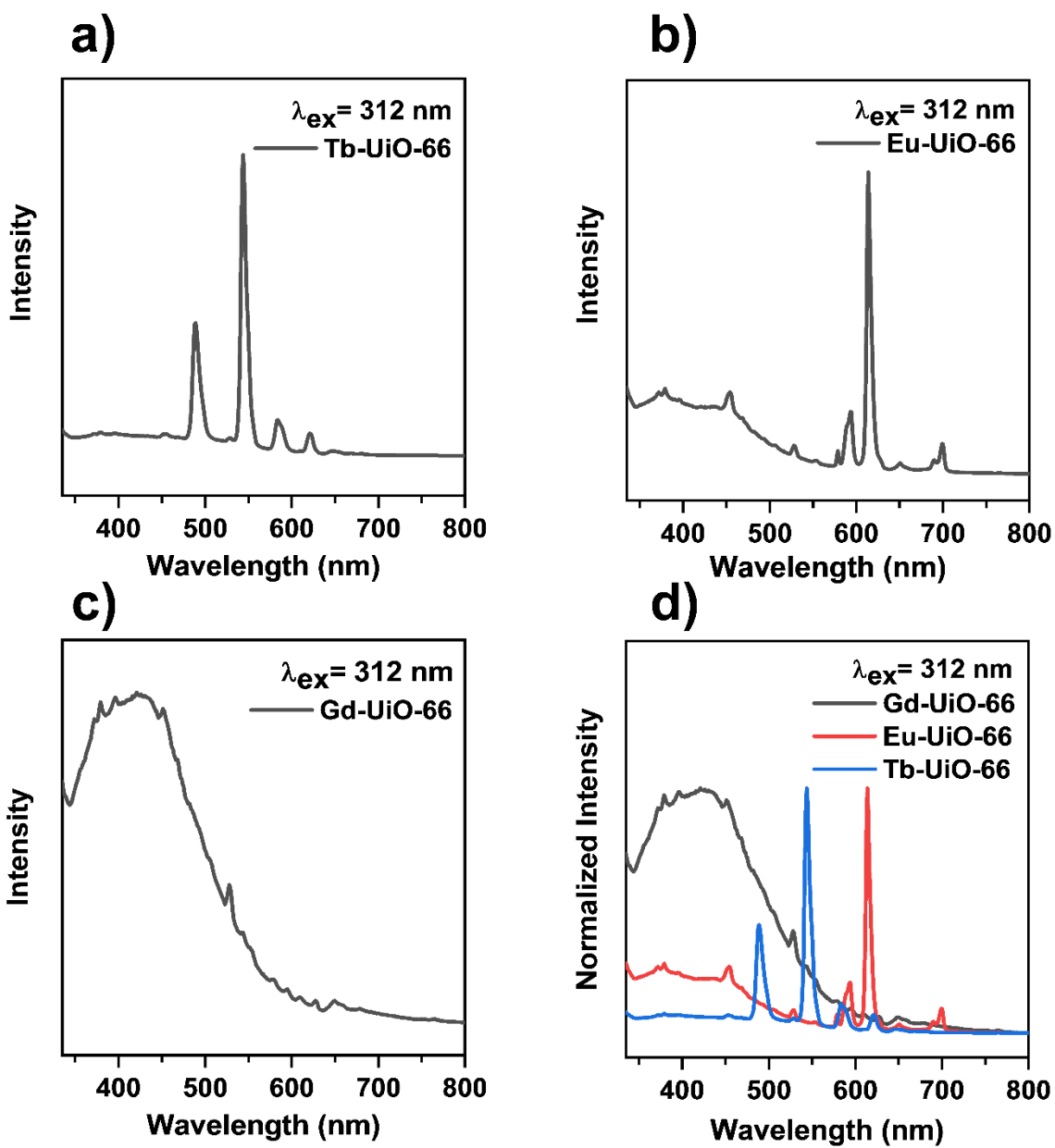


**Figure S7.** Photoluminescence emission spectra of (a) Tb-UiO-66, (b) Eu-UiO-66, (c) Gd-UiO-66, and (d) the normalized emission spectra of (a), (b) and (c).

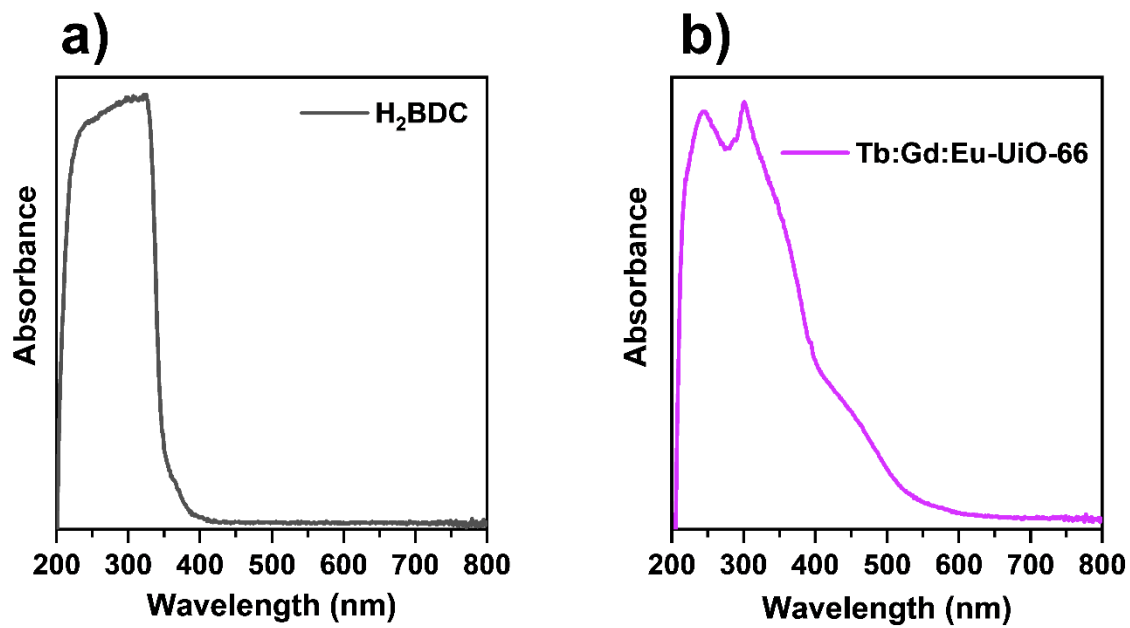


**Figure S8.** Diffuse reflectance UV-Vis spectrum of (a) H<sub>2</sub>BDC and (b) Tb:Gd:Eu-UiO-66.

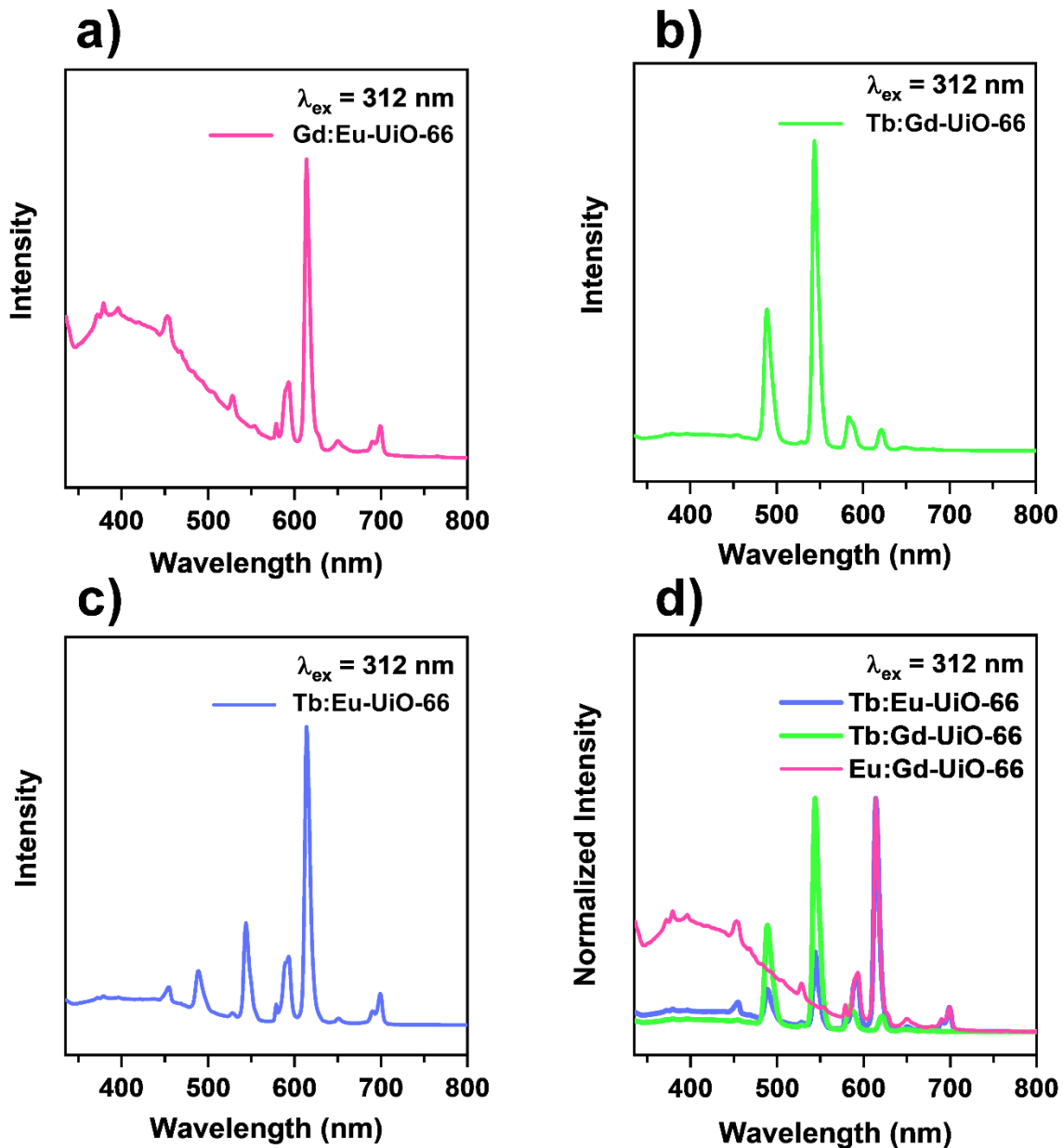


**Figure S9.** Photoluminescence emission spectra of (a) Gd:Eu-UiO-66, (b) Tb:Gd-UiO-66, (c) Tb:Eu-UiO-66, and (d) the normalized emission spectra of (a), (b) and (c).

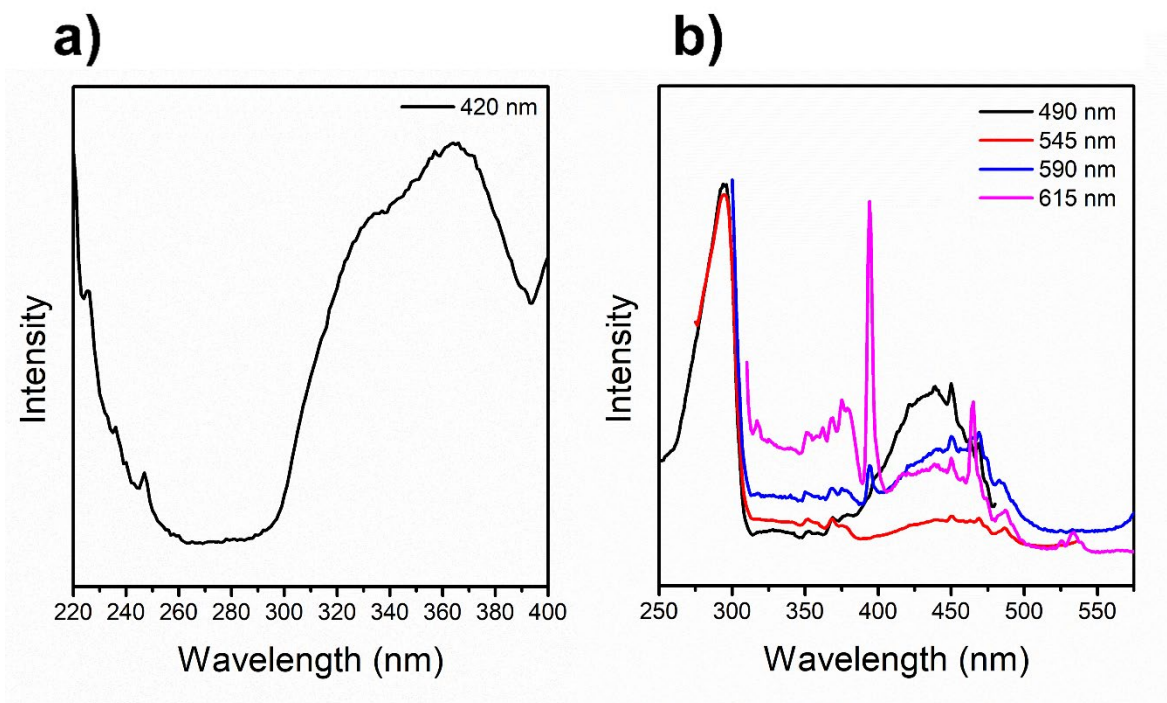


**Figure S10.** Excitation spectra of Tb:Gd:Eu-UiO-66 corresponding to (a) linker-based emission at 420 nm and (b) metal-based emission at 490, 545, 590, and 615 nm.

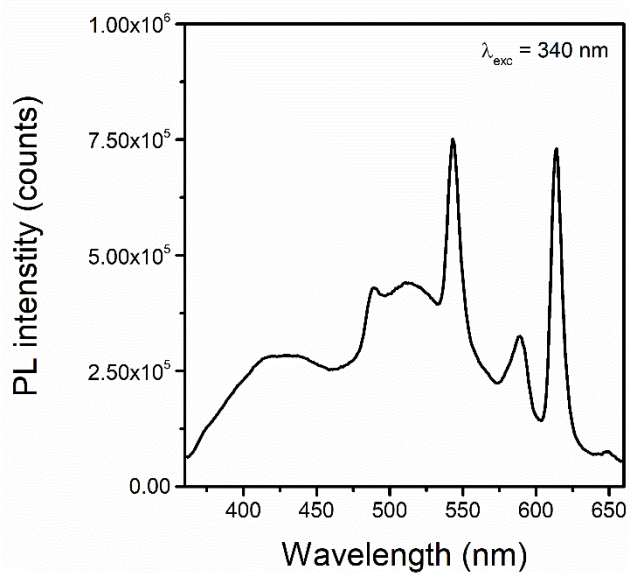


**Figure S11.** Photoluminescence emission spectra of Tb:Gd:Eu-UiO-66 used to calculate the absolute quantum yield (QY = 11.4 %).

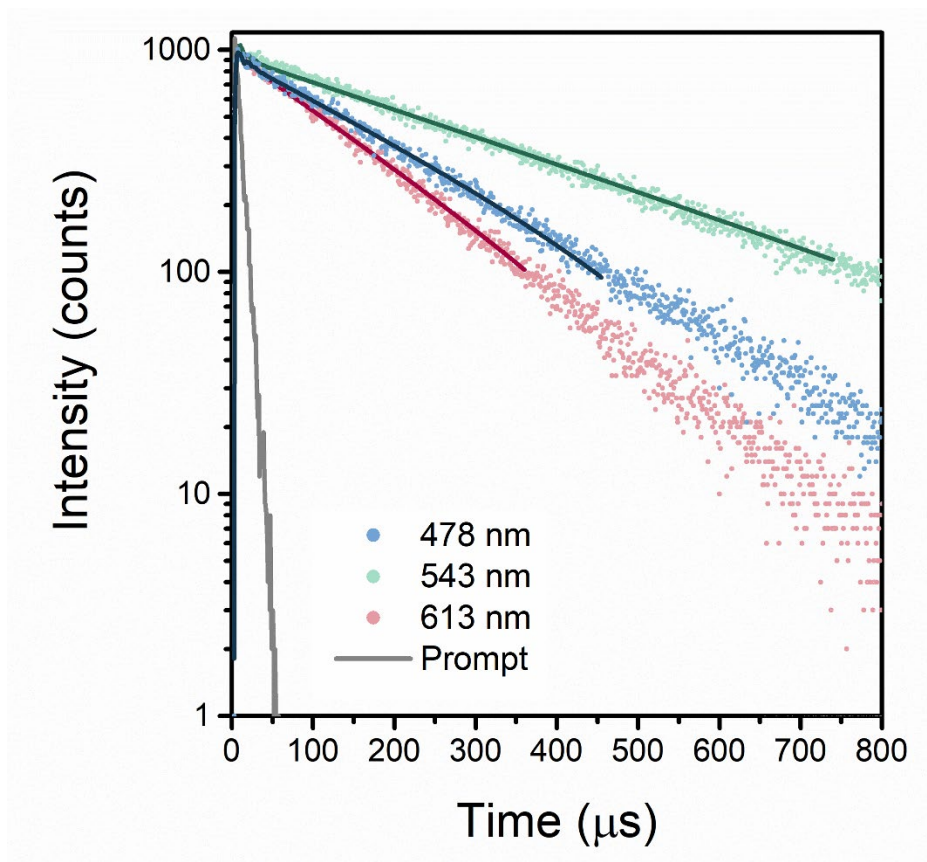


**Figure S12.** Time-resolved fluorescence decay curves measured at different emission wavelengths for Tb:Gd:Eu-UiO-66 ( $\lambda_{exc} = 368$  nm).

**Table S4.** Lifetimes obtained from time-resolved fluorescence decay measurements including the average lifetime at different emission wavelengths for Tb:Gd:Eu-UiO-66.

Wavelength	B <sub>1</sub>	t <sub>1</sub> , s	B <sub>2</sub>	t <sub>2</sub> , s	<t>, s
478 nm	9.04E-01	1.18E-06	9.73E-02	2.35E-04	2.25E-04
543 nm	5.57E-01	1.76E-06	9.68E-02	3.59E-04	3.49E-04
613 nm	9.15E-01	1.22E-06	9.70E-02	1.73E-04	1.62E-04

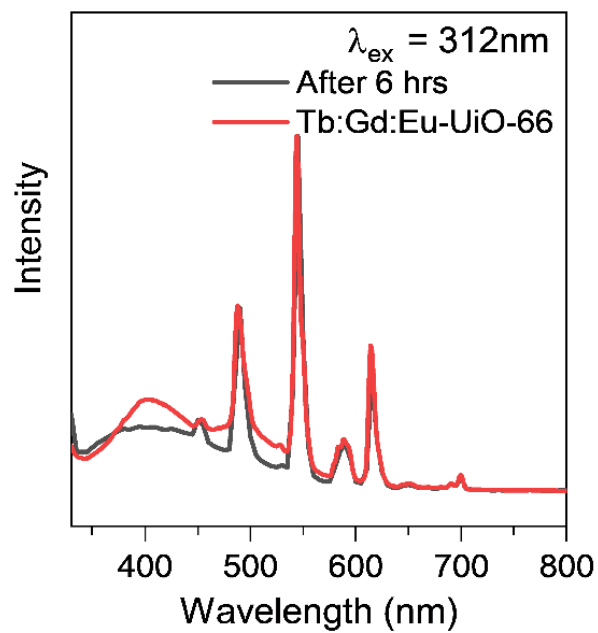


**Figure S13.** Photoluminescence emission spectra of Tb:Gd:Eu-UiO-66 (red trace) and Tb:Gd:Eu-UiO-66 after exposure to 312 nm for 6 hours (black trace).

## References

1. G. M. Sheldrick, *Acta Cryst. C.*, 2015, C71, 3–8.
2. G. M. Sheldrick, *Acta Cryst. A.*, 2015, A71, 3–8.
3. A. L. Spek, *Acta Cryst. C.*, 2015, C71, 9– 18.